Effect of Concentration Quenching on Fluorescence Recovery after Photobleaching Measurements

Julie L. Robeson and Robert D. Tilton
Department of Chemical Engineering, Carnegie Mellon University, Pittsburgh, Pennsylvania USA 15213-3890

ABSTRACT Standard analysis of fluorescence recovery after photobleaching (FRAP) data is valid only if the quantum yield of unphotobleached fluorophores is independent of concentration, yet close molecular packing in two-dimensional systems may lead to significant fluorescence concentration quenching. Using total internal reflection fluorescence, we quantified the surface concentration dependence of the relative quantum yield of fluorescein isothiocyanate–labeled proteins adsorbed to polymeric surfaces before performing measurements of fluorescence recovery after pattern photobleaching. Adsorbed layers of FITC-labeled ribonuclease A displayed significant concentration quenching, and thus the standard FRAP analysis method was unacceptable. We present an extended FRAP analysis procedure that accounts for the changing quantum yield of diffusing fluorophores in systems that are influenced by concentration quenching. The extended analysis shows that if concentration quenching conditions prevail, there may be significant error in the transport parameters obtained from FRAP measurements by using the standard procedures.

INTRODUCTION

With the capability of probing transport over length scales as small as a few micrometers, fluorescence recovery after photobleaching (FRAP) is particularly well suited for measuring slow diffusion and diffusion in confined regions. This technique is therefore frequently applied to biological systems (e.g., Golan and Veatch, 1980; Jacobson and Wojcieszyn, 1984; Elson, 1986; Koppel, 1986), most commonly the cell membrane and cytoplasm. It also has been applied to Langmuir–Blodgett films (Weiss et al., 1982; Wright et al., 1988; Pachence et al., 1990), polymer films (Smith, 1982), and lipid bilayers (Smith et al., 1979) as well as to proteins adsorbed at the solid–liquid interface (Burghardt and Axelrod, 1981; Tilton et al., 1990a,b; Rabe and Tilton, 1993; Gaspers et al., 1994). General procedural issues and several FRAP applications are discussed in detail elsewhere (Axelrod et al., 1976; Thompson et al., 1981; Elson, 1985).

There are several variants of FRAP, but all are based on the irreversible photobleaching reaction that occurs when common fluorophores are exposed to high-intensity excitation light, typically provided by a laser. A photobleaching pulse of high-intensity light superimposes a concentration gradient of functional (i.e., unphotobleached) fluorophores upon an otherwise uniform distribution of labeled molecules. The subsequent relaxation of this gradient is detected by monitoring the fluorescence signal using low-intensity excitation. The transport parameters are calculated from the kinetics of the fluorescence recovery or redistribution as the gradient relaxes. In most cases, these parameters are the self-diffusion coefficient D, and the mobile fraction f. To calculate the transport parameters accurately, one must properly relate the fluorescence intensity to the fluorophore concentration. It is generally assumed that the fluorescence emission is directly proportional to the fluorophore concentration:

$$F(t) \propto \int I(r, \theta)C(r, \theta, t)\mathrm{d}A. \quad (1)$$

$F(t)$ is the time-dependent fluorescence intensity when the sample containing a time-dependent concentration profile of unbleached fluorophores, $C(r, \theta, t)$, is illuminated with an intensity profile $I(r, \theta)$. The integration is performed over the entire illuminated area. The assumption implicit in Eq. 1, that the fluorescence quantum yield is constant, is invalid if fluorescence concentration quenching occurs.

Concentration quenching is a manifestation of the Förster nonradiative energy transfer phenomenon (Förster, 1959; Stryer, 1978), and it is characterized by a decrease in the fluorescence quantum yield as the fluorophore concentration is increased. Nonradiative energy transfer is perhaps most familiar in the context of donor–acceptor energy transfer, where the donor and acceptor are different species. Yet, many fluorophores satisfy the requirement for self-energy transfer (energy transfer between like fluorophores) that there be overlap of the fluorophore's excitation and emission spectra. The efficiency of energy transfer, E, is described by

$$E = \frac{r^{-6}}{r^{-6} + R_0^{-6}}, \quad (2)$$

where r is the interfluorophore separation and R_0 is the Förster radius (Stryer, 1978). R_0 depends on the spectral overlap, the refractive index of the medium, and the relative orientations of fluorophores. Because of the rapid decay of the energy transfer efficiency with increasing r, concentration quenching is significant when r is less than or comparable to R_0. Under concentration quenching conditions, the

Received for publication 20 September 1994 and in final form 6 January 1995.

Address reprint requests to Dr. Robert D. Tilton, Department of Chemical Engineering, Carnegie Mellon University, Pittsburgh, Pennsylvania 15213-3890. Tel.: 412-268-8168; FAX 412-268-7139; *E*-mail: tilton@andrew.cmu.edu.

0006-3495/95/05/2145/11 $2.00

quantum yield is strongly concentration dependent, and it therefore will vary continuously with time and position as the fluorophore concentration profile relaxes during a FRAP measurement. In such cases, the quantum yield must be brought inside the integral of Eq. 1:

$$F(t) \propto \int I(r, \theta)C(r, \theta, t)q_r(C)\mathrm{d}A. \quad (3)$$

The relative quantum yield q_r is the ratio of the quantum yield at concentration C to that at infinite dilution where energy transfer does not occur. Because q_r depends on C, it is of course time and position dependent. It is necessary to measure the dependence of q_r on C in an independent experiment before analyzing FRAP data. It is not necessary to measure the absolute quantum yield or the Förster radius. In this paper we present an extended FRAP analysis procedure to account for concentration quenching effects, and we consider the magnitude of the error that results from applying Eq. 1 to FRAP data under concentration quenching conditions. Under certain conditions, this error may be large and force the more complete FRAP analysis.

We use a fluorescence recovery after pattern photobleaching (FRAPP) version of the technique (see, for example, Weiss et al., 1982; Smith, 1982) to measure the self-diffusion coefficient and mobile fraction of proteins irreversibly adsorbed (strongly bound) to polymeric surfaces. Our instrument operates in a total internal reflection configuration (Tilton et al., 1990a), using an evanescent interference fringe pattern for the FRAPP measurements (TIRFRAPP). The analysis that we present is specific to FRAPP measurements employing sinusoidal illumination patterns for both photobleaching and subsequent low-intensity fluorescence excitation during the recovery stage, but it is easily generalized to other excitation intensity profiles.

THEORY

In fringe pattern photobleaching two equal-intensity, coherent laser beams are intersected to form a periodic fringe pattern with the sinusoidal intensity profile

$$I(x) = I_0\,(1 + A\sin(\pi x/w)), \quad (4)$$

where $I(x)$ is the local laser intensity, I_0 is the incident laser intensity, A is the experimentally determined amplitude of the laser fringe pattern, and w is the half-period of the fringe pattern. Because of the large aspect ratio of the fringes typically used, only diffusion in the direction perpendicular to the fringes contributes significantly to the fluorescence recovery dynamics. Therefore, w is the characteristic length scale for diffusion.

For one-dimensional diffusion along the x axis, the fluorescence signal described by Eq. 3 simplifies to

$$F(t) \propto \int_{-w}^{w} I(x)C(x, t)q_r(C)\mathrm{d}x. \quad (5)$$

The following analysis of $F(t)$ is the standard analysis for a fringe pattern FRAPP measurement where concentration quenching is neglected and is similar to those of Abney et al. (1992) and Tilton et al. (1990a). The unbleached fluorophore concentration profile $C(x,t)$ is governed by the one-dimensional diffusion equation:

$$\frac{\partial C}{\partial T} = \frac{\partial^2 C}{\partial X^2}, \quad (6)$$

where

$$X = x/w \quad (7a)$$

and

$$T = \frac{Dt}{w^2}. \quad (7b)$$

The first-order photobleaching reaction (Axelrod et al., 1976) establishes the initial condition as

$$C(X, 0) = \bar{C}e^{-kI(X)}, \quad (8)$$

where $\bar{C}$ is the uniform, prebleach concentration of fluorophores and $I(X)$ is the photobleaching intensity profile $(1 + A\sin \pi x/w)$. k includes the rate constant for photobleaching and the duration and intensity of the photobleaching pulse and therefore serves as an index to the extent of photobleaching. The concentration profile

$$C(X, T) = \frac{a_0}{2} + \sum_{n=1}^{\infty} \exp(-n^2\pi^2 T)\,[a_n \cos(n\pi X) + b_n \sin(n\pi X)] \quad (9)$$

satisfies Eqs. 6–8. Here, a_n and b_n are Fourier coefficients, given by

$$a_n = \int_{-1}^{1} \exp(-kI(X))\cos(n\pi X)\mathrm{d}X, \quad (10)$$

$$b_n = \int_{-1}^{1} \exp(-kI(X))\sin(n\pi X)\mathrm{d}X, \quad (11)$$

and depend only upon k.

When fluorescence concentration quenching is not present, $q_r = 1$ for all fluorophore concentrations. In this case, substituting Eqs. 9 and 7 into relation 5 yields the following for $F(t)$:

$$F(t) \propto I_0\bar{C}a_0 w + AI_0\bar{C}b_1 w \exp\left(-\pi^2\frac{Dt}{w^2}\right), \quad (12)$$

where either all other Fourier coefficients besides a_0 and b_1 are zero or the terms containing them drop out upon integration. Relation 12 applies strictly to the case where all fluorescent molecules are mobile. Allowing for a heterogeneous population of molecules consisting of a mobile fraction capable of diffusion, f, and a fraction that is immobile

on the time scale of the experiment, $1-f$, relation 12 becomes

$$F(t) \propto I_0 \bar{C} a_0 w + (1-f) A I_0 \bar{C} b_1 w + f A I_0 \bar{C} b_1 w \exp\left(-\pi^2 \frac{Dt}{w^2}\right). \quad (13)$$

Using relation 5, again with $q_r = 1$, we obtain expressions for the fluorescence intensity before photobleaching, $F(t < 0) = \bar{F}$, and immediately after photobleaching, $F(t = 0) = F_0$:

$$\bar{F} \propto 2 I_0 \bar{C} w, \quad (14)$$

$$F_0 \propto I_0 \bar{C} w (a_0 + A b_1). \quad (15)$$

Given the assumption of a constant quantum yield, the proportionality constants implied in relations 13–15 are all identical, and we can combine these expressions to eliminate I_0, $\bar{C}$, and the unknown proportionality constant. The fluorescence recovery is thus described by

$$F(t) = (F_0 - \bar{F}) \left\{1 - \frac{A b_1 f}{2 - a_0 - A b_1}\left[1 - \exp\left(-\frac{\pi^2 D t}{w^2}\right)\right]\right\} + \bar{F}, \quad (16)$$

where the only unknowns are D and f. These are determined by a nonlinear least-squares regression of Eq. 16 to the experimental $F(t)$ data. k, a_0, and b_1 are not unknowns; we determine them directly in each experiment from the measured values of F_0 and $\bar{F}$ by using Fig. 1 and Eqs. 10 and 11. Note that, in order to check the regressed value of the mobile fraction, f also may be calculated directly from Eq. 16 in the limit as $t \to \infty$:

$$f = \frac{2 - a_0 - A b_1}{A b_1}\left(\frac{F(\infty) - F_0}{\bar{F} - F_0}\right). \quad (17)$$

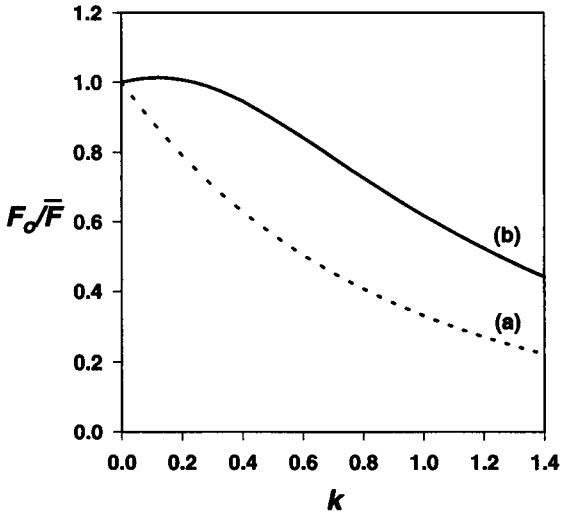

FIGURE 1 The ratio of the fluorescence intensity immediately after the photobleaching pulse to the intensity before photobleaching, $F_0/\bar{F}$, is used to determine the photobleaching parameter k for (a) a system free from concentration quenching effects and (b) a system where concentration quenching is significant. (Curve (b) was generated for FITC-ribonuclease A adsorbed to polystyrene, $\Gamma = 0.22$ μg/cm^2, and a labeling ratio $L = 0.10$ mole FITC/mole protein.) The Fourier coefficients a_n and b_n are calculated from Eqs. 10 and 11 by using this graphically determined value of k.

Effects of concentration quenching

Expressions 13–17 are valid only for $q_r = 1$. When fluorescence concentration quenching is present, q_r becomes a function of fluorophore concentration. The explicit dependence of q_r on C, i.e., the functional form of $q_r(C)$, must then be determined experimentally and substituted into relation 5 for numerical evaluation of $F(t)$, F_0, and $\bar{F}$.

First we create a new plot of $F_0/\bar{F}$ versus k, using the experimentally determined $q_r(C)$ relationship (for example, Fig. 1, curve b) as follows. From relation 5, we numerically calculate F_0 over a range of k values, using $q_r(C(X, 0))$ (see relation 20) and $C(X, 0)$ from Eq. 8, and we numerically calculate $\bar{F}$ using $C = \bar{C}$ and $q_r(\bar{C})$. This makes it possible to determine k from measurements of $F_0/\bar{F}$ and thereby to calculate the Fourier coefficients a_n and b_n by using Eqs. 10 and 11, for each experiment. The fluorescence recovery $F(t)$ is calculated numerically, using relation 5, with $q_r(C(X, T))$, where $C = C(X, T)$ is given by Eq. 9 and the appropriate Fourier coefficients. This concentration profile (Eq. 9) is valid in both the presence and the absence of concentration quenching (the only difference being the values of the Fourier coefficients calculated from the data) because the same initial condition, Eq. 8, holds in either case. Just as in the standard analysis, the diffusion coefficient and the mobile fraction are determined by nonlinear regression of experimental fluorescence recovery data.

Curve b in Fig. 1 shows a plot of $F_0/\bar{F}$ versus k corrected for the $q_r(C)$ relationship for adsorbed fluorescein isothiocyanate- (FITC-) labeled ribonuclease A (RNase A) measured in the current work. (The experimental procedure to determine the functionality of $q_r(C)$ is described later.) Because the $q_r(C)$ dependence is unique to each system, we present no universal analytical expression to be applied to FRAPP measurements when concentration quenching is important. Any $q_r(C)$ dependence may be accommodated by the general procedure described above.

MATERIALS AND METHODS

Protein

Bovine serum albumin (BSA, essentially fatty acid free, A-7511, Sigma) was fluorescence labeled with FITC (Molecular Probes) by standard procedures (Lok et al., 1983a), substituting a sodium borate decahydrate buffer for the carbonate buffer. We reacted a 1:1 molar ratio of FITC to BSA to ensure that the labeling ratio (L = moles FITC/mole protein) could never exceed 1. Unreacted FITC was removed from the labeled BSA by size exclusion chromatography, using a Bio-Gel P6 column (Bio-Rad). The column was pre-equilibrated with 0.05 M, pH 8.0 triethanolamine buffer, the solution used for the adsorption experiments. The concentration of the stock BSA solution and the labeling ratio were determined spectrophotometrically by using the extinction coefficients $\epsilon_{BSA}^{278} = 44{,}890$ M^{-1} cm^{-1}, $\epsilon_{FITC}^{278} = 18{,}180$ M^{-1} cm^{-1}, and $\epsilon_{FITC}^{492} = 66{,}350$ M^{-1} cm^{-1}. The labeling ratio was 0.86 ± 0.07 and was decreased in experiments by dilution with unlabeled BSA.

To dissociate dimers in the commercial preparation, we dialyzed bovine pancreatic RNase A (Type IIA, Sigma) against pH 6.5 phosphate-buffered saline solution (PBS) for 2 h with stirring and subsequently heated it at 62°C for 10 min (Fruchter and Crestfield, 1965; Norde and Lyklema, 1978). We then separated the protein into two fractions. The fraction to be fluorescence labeled we dialyzed with stirring for 2 h against pH 9.0 sodium borate decahydrate solution. By measuring the change in pH, we determined that 2 h was sufficient for 5 ml of pH 6.5 phosphate-buffered saline inside the dialysis bag to be replaced by pH 9.0 sodium borate decahydrate solution. We reacted 0.75 mol FITC per mole of RNase A for 1 h and separated the labeled protein from unreacted FITC in the Bio-Gel P6 size exclusion chromatography column. The unlabeled fraction was simply dialyzed for 2 h against the solution to be used in the experiment, either 0.05 M, pH 6.0 KNO_3 (for experiments with polydimethylsiloxane surfaces) or 0.05 M, pH 8.0 triethanolamine buffer (for experiments with polystyrene surfaces). The labeling ratio determined spectrophotometrically, using $\epsilon^{278}_{RNase} = 9{,}410\ M^{-1}\ cm^{-1}$, $\epsilon^{278}_{FITC} = 18{,}180\ M^{-1}\ cm^{-1}$, and $\epsilon^{492}_{FITC} = 66{,}350\ M^{-1}\ cm^{-1}$, was 0.5 ± 0.1. All water used in this investigation was deionized and purified in a MilliQ Plus (Millipore) unit.

Adsorption Substrates

All adsorption substrates were polymer films that were spin cast onto copiously cleaned microscope slides or silicon wafers. To improve adhesion of polystyrene films during prolonged exposure to aqueous solutions, we found it necessary to hydrophobize the substrate by silanization before spin casting.

Before silanization and/or spin casting, we cleaned microscope slides (3 × 1 in., Gold Seal) by the method of Cheng et al. (1987), and we cleaned silicon wafers (3 × 2 inches, Lattice Materials Corp.), bearing a ~2-nm native oxide layer, in RBS (Pierce) detergent solution. We then immediately spin cast polydimethylsiloxane (PDMS, silanol terminated, Hüls) films from a 1-wt. % solution in heptane containing 0.01-wt. % stannous octoate (Hüls) as a cross-linking catalyst. We placed the substrates under a heat lamp for 1 h to cross-link the polymer and to ensure complete evaporation of heptane. Before spin-coating the polystyrene films, we used a simple vapor phase silanization method wherein the substrates were held in a saturated atmosphere of trimethylchlorosilane (Petrarch) and water in a desiccating jar for 30 min. We then rinsed the substrates with ethanol to remove any unreacted silane, dried them with a jet of high-purity nitrogen gas, and placed them under a heat lamp for 10 min to ensure complete drying. After the substrates cooled to room temperature, they were immediately spin cast with polystyrene (MW = 125,000–150,000, Polysciences) from 1-wt. % solutions in toluene and allowed to dry under a heat lamp for 1 h.

Protein surface concentration determination

We measured the adsorbed protein surface concentration by scanning angle reflectometry (Schaaf et al., 1987), using polymer-coated silicon wafers as the reflective substrate. It was necessary to measure the thickness of the spin-cast polymer layer before the adsorption of protein. This thickness was determined at several different points on the surface to check for film uniformity. The PDMS and polystyrene films were 20 ± 1 and 30 ± 1 nm thick, respectively. We adsorbed the protein from flowing solutions (50 μg/ml for the RNase A experiments and 100 μg/ml for the BSA experiments) onto the polymeric substrates for 4–6 h. We then determined the thickness and the refractive index of the adsorbed layer optically and calculated the surface concentration Γ from those values, using

$$\Gamma = \frac{(n_1 - n_0)d_1}{dn/dc}, \tag{18}$$

where n_0 is the refractive index of the solution and n_1 and d_1 are the refractive index and the thickness of the protein layer, respectively. The refractive-index increment, dn/dc, is 0.18 cm^3/g for proteins.

TIRFRAPP

Total internal reflection fluorescence (TIRF) employs an evanescent wave to excite fluorescence in molecules adsorbed at interfaces. We use this surface-sensitive technique to monitor the evolution of the fluorescence signal as labeled proteins adsorb to the surface before photobleaching. TIRF is described in detail elsewhere (Lok et al., 1983a,b).

The TIRFRAPP apparatus is a modification of that described by Tilton et al. (1990a). The most significant modifications include computer-controlled electronic shutters, to control precisely the duration of the photobleaching pulse, and a piezoelectrically driven mirror (see Fig. 2) that provides the option of oscillating the monitoring fringe pattern over the underlying photobleached pattern. We used the fringe pattern oscillation to measure the amplitude of its sinusoidal intensity profile, as described below. We conducted FRAPP measurements without oscillating the fringes. A FRAPP recovery curve typical of a protein monolayer with a low density of fluorophores is illustrated in Fig. 3.

In preparation for each TIRFRAPP experiment, we first degassed the aqueous, protein-free solution under vacuum and then added predetermined volumes of unlabeled and labeled protein stock solutions to obtain the desired labeling ratio and total protein concentration (either 50 μg/ml for the RNase A experiments or 100 μg/ml for the BSA experiments). We conducted all experiments at 25°C, maintained by circulating constant-temperature water through the flow cell casing. Before contacting with protein solution, we filled and rinsed the flow cell with degassed protein-free solution for 10 min. We then began the flow of protein solution and measured the fluorescence signal as proteins adsorbed. At the end of the adsorption step, we rinsed the flow cell with unlabeled protein solution to remove all labeled proteins from the bulk solution and any labeled proteins that were only loosely associated with the adsorbed layer. After rinsing, the fluorescence signal rapidly dropped to a slightly lower value $\bar{F}$ that remained constant over long periods of time (at least 1 order of magnitude longer than the time required for a typical FRAPP measurement). This ensured that only tightly adsorbed proteins contributed to the fluorescence signal during photobleaching measurements. We conducted all FRAPP diffusion measurements after steady-state adsorption had been reached. By translating the sample stage, we photobleached an average of 12 spots per substrate in a given experiment.

Measuring the amplitude of the fringe pattern

Ideally, the amplitude of the incident interference fringe pattern, A in Eq. 4, should be unity. In practice it may be less than unity if the two intersecting

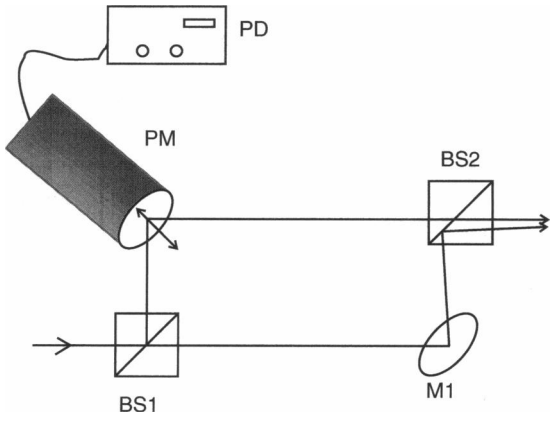

FIGURE 2 The interferometer used to produce the fringe pattern consists of two 50:50 beamsplitters (BS1 and BS2) and two mirrors (M1 and PM) to separate the incoming beam into two equal-intensity beams and to control their angle of intersection at the point of total internal reflection in the flow cell. One mirror (PM) is mounted on a piezoelectric positioner that may be driven by a function generator-controlled power supply (PD). Thus, the position of PM can be made to oscillate in the direction shown by the arrow.

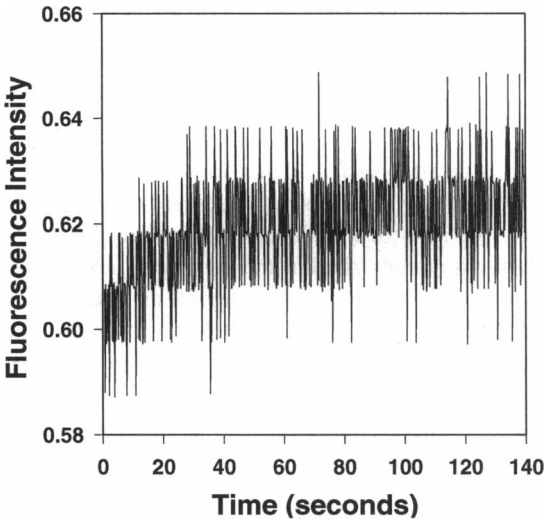

FIGURE 3 FRAPP recovery curve typical of a tightly bound protein monolayer with a low density of fluorophores and low mobile fraction, obtained with FITC-labeled bovine serum albumin irreversibly adsorbed from pH 8.0 triethanolamine buffer solution to a polystyrene surface.

beams are not of precisely equal intensity or if they are not perfectly coherent. In addition, the nature of optical interference in evanescent waves is such that the amplitude of evanescent fringe patterns may be less than unity, depending on the angle of the laser beam incidence to the solid–liquid interface (Abney et al., 1992), although this is not a major factor for the laser beam angles used in our instrument.

We measured the amplitude of the sinusoidal fringe pattern by photobleaching it onto a surface containing *immobile* fluorophores and then oscillating the low-intensity monitoring fringe pattern to measure the contrast in fluorescence between the peaks and valleys of the periodic fluorophore distribution on the surface. After photobleaching, a maximum in the fluorescence signal (F_{180}) was observed when the phase of the monitoring fringes was shifted 180° so that they were in phase with the fluorophore concentration profile (see Fig. 4). Similarly, a minimum in the fluorescence signal (F_0) was observed when the monitoring fringes were not shifted, and they were thus completely out of phase with the underlying photobleached pattern. We used the difference between these two fluorescence intensities

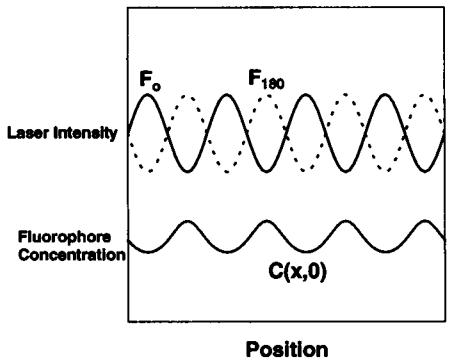

FIGURE 4 The fluorophore concentration profile and the monitoring laser fringe pattern intensity profiles. $C(x,0)$ is the fluorophore concentration distribution after the photobleaching pulse. The minimum fluorescence intensity F_0 is observed when the monitoring fringe pattern has not been shifted (——), while the maximum signal F_{180} is observed when the fringe pattern has been shifted into phase (- - - -) with the underlying fluorophore concentration profile $C(x,0)$. During FRAPP measurements, the fringe pattern is not shifted.

to calculate A. We did this iteratively by first assuming a value for A in expressions 4 and 5 to generate plots of $F_0/\bar{F}$ and $(F_0 - F_{180})/\bar{F}$ versus k. If the experimentally measured values of $F_0/\bar{F}$ and $(F_0 - F_{180})/\bar{F}$ were both correctly predicted at the same value of k, the assumed value of A was correct. If not, a new value for A was assumed and the procedure repeated. As a further check, we used several different photobleaching pulse durations (different values of k) to verify that the same value of A was satisfactory in every case. Fig. 5 shows the resultant plot for the correct value of the amplitude, $A = 0.61$. This procedure also confirmed the proper alignment of the photobleaching and monitoring fringe patterns.

The immobilized fluorophore system consisted of FITC (1.5×10^{-5} M) bound to a 20-wt. % solution of Knox gelatin in pH 9.0 sodium borate decahydrate solution. We allowed the FITC to react with the gelatin for 1 h. Before gelation, it was spin cast onto precleaned microscope slides and allowed to gel overnight in a humid atmosphere to minimize water loss. This slide was then placed in the TIRFRAPP cell for photobleaching in the total internal reflection configuration. Because concentration quenching in three-dimensional solutions is insignificant at concentrations below 10^{-3} M (Förster, 1959), this measurement is free from concentration quenching artifacts. Using a gel with high water content also preserved the conditions necessary for total internal reflection at the substrate–water interface.

RESULTS AND DISCUSSION

Detection of concentration quenching

The occurrence of concentration quenching may not be obvious in a FRAPP measurement, because the recovery curves retain their qualitative shape. To detect and quantify the effects of concentration quenching, we combine FRAPP with TIRF. The latter allows us to monitor the development of the fluorescence signal throughout the entire adsorption process and can serve as a flag for concentration quenching. As shown in Fig. 6 for FITC-RNase A adsorbing to polystyrene, the fluorescence signal passed through a maximum and decreased as the surface concentration of labeled proteins increased over time. This "overshoot" in the fluorescence signal is explained by the competition between a simple increase

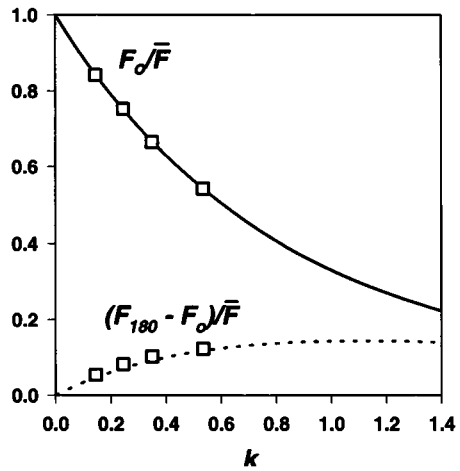

FIGURE 5 Comparison of maximum and minimum fluorescence intensities observed as the monitoring fringe pattern is oscillated after photobleaching an immobile sample reveals the amplitude of the (fringe pattern) incident intensity profile A. The ratios $F_0/\bar{F}$ and $(F_{180} - F_0)/\bar{F}$ are *both* predicted correctly only when the value of A is correct. Different photobleaching durations were used to check the consistency of the value determined for A. The data (□) indicate that $A = 0.61$.

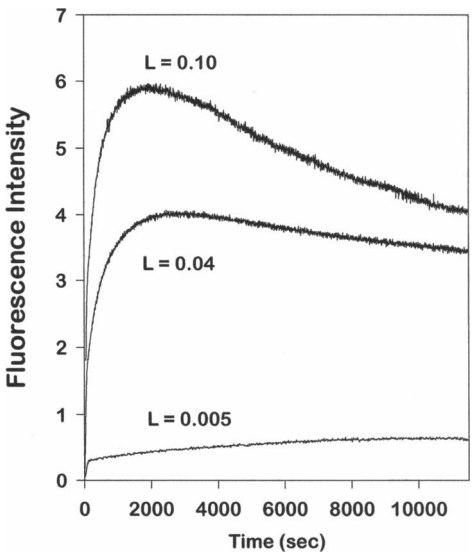

FIGURE 6 At higher labeling ratios, the TIRF signal passed through a maximum as FITC-RNase A adsorbed to polystyrene, indicating the presence of concentration quenching. No concentration quenching was observed at the lowest labeling ratio, $L = 0.005$.

in the number of fluorophores at the interface and the consequent decrease in quantum yield of each of those fluorophores as the average interfluorophore separation approaches R_0. Larger labeling ratios therefore produced more dramatic overshoots and signal maxima that occurred at earlier times. For the lowest labeling ratio, $L = 0.005$, the surface concentration of fluorophores was never sufficiently large for concentration quenching to occur, and consequently there was no overshoot. This TIRF trace at $L = 0.005$ is an accurate representation of the protein adsorption kinetics. Although slow photobleaching by the monitoring beam may produce TIRF overshoots, the results presented here are not due to slow photobleaching. We ruled out photobleaching by performing the same adsorption experiments with only brief, periodic exposures to the monitoring beam. The time dependence of the fluorescence signal was in all cases identical to that observed with continuous exposure to the monitoring beam.

Using Eq. 2, we may estimate the efficiency of energy transfer to support the conclusion that concentration quenching was responsible for the fluorescence overshoot. We used scanning angle reflectometry to determine that the surface concentration of adsorbed RNase A was 0.22 ± 0.02 μg/cm^2 on polystyrene, corresponding to an average interfluorophore separation of 260 Å for a labeling ratio of 0.005. For this simple comparison, we make the (questionable) assumption that R_0 for self-energy transfer between fluoresceins covalently attached to adsorbed proteins is comparable with that for fluorescein freely rotating in solution (50 Å). A 260-Å interfluorophore separation then would correspond to a self-energy transfer efficiency of only 5×10^{-5}, and no overshoot should be expected. For comparison, the average interfluorophore separation for a labeling ratio of 0.10 is 57 Å, and the efficiency of energy transfer is significant, approximately 30%.

Determination of the relative quantum yield

If one measures the surface concentration dependence of the relative quantum yield, it is not necessary to know the value of R_0 for the adsorbed FITC-labeled protein. We measured the relative quantum yield of the adsorbed, labeled proteins by recording TIRF fluorescence signals as a function of the labeling ratio. For RNase A, we held the bulk protein concentration constant at 50 μg/ml, but we varied the labeling ratio between 0.005 and 0.25 in different experiments by diluting a standard stock solution with unlabeled proteins. FITC–RNase A was allowed to adsorb for a time sufficient to reach a steady surface concentration, as indicated by the TIRF kinetic data obtained with the lowest labeling ratio. Fig. 7 *a* shows that the fluorescence intensity emitted by the saturated adsorbed FITC-RNase A layer does not increase linearly with increasing labeling ratio. If we assume that the average labeling ratio on the surface equals that in solution, the surface concentration of fluorophores (C) is simply the product of the protein surface concentration obtained from scanning angle reflectometry and the appropriate labeling ratio. (Experiments supporting this assumption are described below.) Thus, we conclude that the fluorescence intensity is not linearly proportional to the surface concentration of fluorophores. The straight line in Fig. 7 *a* is a linear regression of the data at low labeling ratios where concentration quenching is apparently insignificant, and it indicates the fluorescence intensities that would be expected in the absence of concentration quenching, i.e., if the quantum yield were constant.

We calculated the relative quantum yield from these data according to

$$q_r(C) = \frac{F(C)}{C\,[dF/dC]_0}, \tag{19}$$

where $F(C)$ is the fluorescence signal at a fluorophore surface concentration C and $(dF/dC)_0$ is the limiting slope as the fluorophore surface concentration approaches zero (i.e., the slope of the line in Fig. 7 *a*). Fig. 8 shows that q_r of the FITC-labeled RNase A decreased monotonically with increasing fluorescein surface concentration on both PDMS and polystyrene surfaces. Because the surface concentration of RNase A on PDMS ($\Gamma = 0.25 \pm 0.02$ μg/cm^2) was similar to that on polystyrene, and the quantum yield of FITC-RNase A displayed a similar concentration dependence for both types of surface, we analyzed both sets of results together to obtain an empirical functional form of the $q_r(C)$ relationship. The sigmoidal relation

$$q_r(C) \approx \frac{0.93}{1 + \exp[30000(C - 6 \times 10^{-5})]} + 0.2 \tag{20}$$

(with C expressed as molecules FITC/Å^2) provides a good description of the concentration quenching results. The sigmoidal form of the $q_r(C)$ dependence is consistent with two-

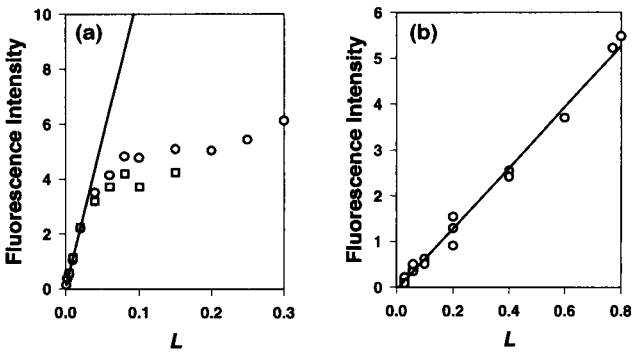

FIGURE 7 (*a*) The fluorescence signal for FITC-RNase A adsorbed to either polystyrene (□) or PDMS (○) surfaces does not vary linearly with the labeling ratio. The units for fluorescence intensity are arbitrary, and the absolute intensities for FITC-RNase A on PDMS were approximately a factor of 10 lower than those on polystyrene because of the lower pH of the solution and a lower excitation intensity used in the PDMS experiments. Those intensities were simply multiplied by a constant so they could be presented on the same graph. This does not affect the determination of *relative* quantum yields. (*b*) The fluorescence signal for FITC-BSA adsorbed to polystyrene is linear in labeling ratio, indicating the absence of concentration quenching.

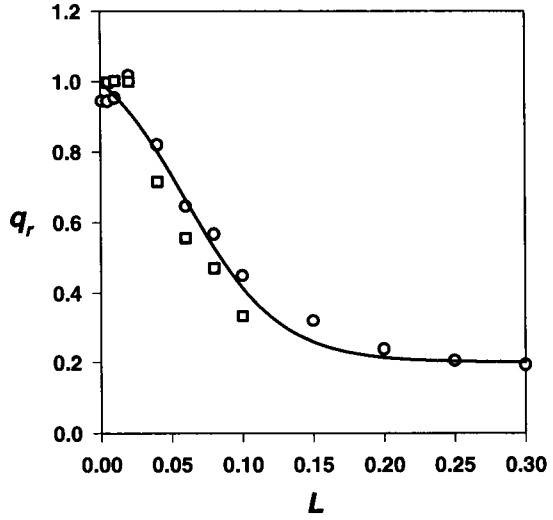

FIGURE 8 The relative quantum yield for FITC-RNase A decreases with increasing labeling ratio, corresponding to increasing fluorophore surface concentration at a constant protein surface concentration. The dependence of the relative quantum yield on surface concentration is similar for FITC-RNase A adsorbed to both polystyrene (□) and PDMS (○) surfaces. The curve is an empirical fit of the results by relation 20.

dimensional fluorescence energy transfer theories (Wolber and Hudson, 1979; Snyder and Freire, 1982).

For comparison, Fig. 7 *b* shows that the fluorescence signal emitted from adsorbed FITC-BSA layers on polystyrene surfaces was directly proportional to the labeling ratio. Thus concentration quenching was absent, and $q_r = 1$ for labeling ratios from 0.03 to 0.8. Using scanning angle reflectometry, we determined that the surface concentration of BSA on polystyrene was 0.13 ± 0.02 $\mu g/cm^2$, so this range of labeling ratios corresponded to average interfluorophore separations of 300 to 60 Å. Unlike adsorbed FITC-RNase A, where concentration quenching was important over most of the labeling ratio range investigated, FITC-BSA concentration quenching should not be expected to be important for any but the highest labeling ratio examined. The key difference between RNase A and BSA is the molecular size. BSA is a much larger molecule than RNase A (67,000 versus 13,700 molecular weight), so similar surface mass concentrations correspond to much higher surface molar concentrations of RNase A than of BSA, and therefore to higher FITC concentrations. In addition, the theory of two-dimensional energy transfer predicts that the distance of closest fluorophore approach influences the energy transfer efficiency (Wolber and Hudson, 1979). The large size of BSA can hinder close fluorophore approach more than is the case with RNase A, resulting in lower energy transfer efficiencies for FITC-BSA even at comparable average interfluorophore separations. Thus, concentration quenching is insignificant for BSA with a labeling ratio as high as 0.8, whereas adsorbed FITC-RNase A is quenched with labeling ratios as low as 0.04. It should also be considered that the Förster radii for adsorbed FITC-BSA and FITC-RNase A may be different because of possible differences in the average fluorophore orientation (Fung and Stryer, 1978). Regarding the usefulness of TIRF adsorption measurements to signal the possible presence of concentration quenching, we note that we observed no TIRF overshoots during adsorption of FITC-BSA, consistent with the absence of concentration quenching.

In quantifying the relative quantum yield, it is important to work with identically prepared protein stock solutions, with constant labeling ratios that are less than 1. The stock solution should also be consistent with those used in subsequent FRAPP measurements. This is necessary because random covalent labeling produces a distribution of the number of fluorophores per protein, and there will be a significant difference in the energy transfer behavior of two fluorophores bound to the same protein as opposed to two fluorophores bound to different proteins.

In order to correct the FRAPP analysis by using the $q_r(C)$ relationship obtained by directly varying the fluorophore surface concentration in this way, we assume that a photobleached fluorophore is spectroscopically equivalent to an unlabeled protein at the wavelengths appropriate for energy transfer. It was previously noted that photobleaching does indeed diminish the fluorophore absorbance at the excitation wavelength (Tilton et al., 1990a; Tilton, 1991), lending support to this assumption. If there is not perfect correspondence between the relief of concentration quenching by photobleaching and by altering the average labeling ratio of the adsorbed protein population, this correction will still be qualitatively, if not quantitatively, correct.

Check for preferential adsorption

We considered the possibility that the nonlinear dependence of the fluorescence intensity on labeling ratio and the TIRF overshoot resulted from preferential adsorption of labeled

RNase A versus unlabeled RNase A, rather than from concentration quenching. In fact, preferential adsorption of labeled protein at the expense of unlabeled protein would reproduce the qualitative behavior of the fluorescence intensity shown in Fig. 7 *a*. In that case, the average labeling ratio on the surface would exceed that in solution. At high labeling ratios, the surface might be overpopulated by labeled proteins. Then, increasing the average labeling ratio in solution would lead to a disproportionately small increase in the surface concentration of fluorophore, and the fluorescence signal would increase by only a small amount, as in Fig. 7. One way to illustrate this behavior is to assign a difference in energy barriers to adsorption, ΔE, that favors adsorption of labeled proteins. Then, even in the absence of concentration quenching, the fluorescence signal would depend on the labeling ratio L as

$$F(L) \propto \frac{Le^{\Delta E/kT}}{1 + L(e^{\Delta E/kT} - 1)}, \qquad (21)$$

assuming that the ratio of labeled versus unlabeled proteins on the surface is given simply by the ratio of their concentrations in solution biased by a Boltzmann distribution. When there is preferential adsorption of labeled proteins, relation 21 displays the concave downward behavior characteristic of the data in Fig. 7. This behavior would be the same regardless of the particular scheme used to represent the bias toward labeled protein adsorption. Thus, to investigate the possibility of preferential adsorption, we conducted a series of TIRF experiments.

We checked for preferential adsorption by comparing the ability of dissolved, labeled RNase A to displace adsorbed, unlabeled RNase A, and vice versa. First, unlabeled RNase A was adsorbed from a 50-μg/ml solution to polystyrene for 3 h. Then, a 50-μg/ml solution of FITC-RNase A with an average labeling ratio of 0.02 was allowed to circulate through the flow cell for 4 h, after which we noted the increase in fluorescence intensity. We examined the ability of unlabeled RNase A to displace FITC-RNase A by reversing these steps and noting the decrease in signal after introducing unlabeled RNase A. It was necessary to use very low labeling ratios for the FITC-RNase A solutions to ensure that concentration quenching could not affect the results. After the 4-h exchange, the fluorescence signal had reached a plateau. The fluorescence intensity changed by $+4800 \pm 1100$ counts when FITC-RNase A displaced unlabeled RNase A and by -4800 ± 800 counts in the reverse case, with similar kinetics in each case. This change in signal represented approximately 25% of the total fluorescence. Thus, there was no preferential adsorption of *either* FITC-labeled RNase A or unlabeled RNase A.

This conclusion is supported further by noting that it is not possible to use preferential adsorption to explain both the TIRF overshoot and the dependence of the fluorescence intensity on the labeling ratio. As noted above, the concave downward form of the fluorescence intensity versus labeling ratio plot would require preferential adsorption of *labeled* RNase A at the expense of unlabeled RNase A, but the overshoot in the TIRF curve would require just the opposite preferential adsorption: To produce the overshoot in the absence of concentration quenching, *unlabeled* proteins would gradually have to displace labeled proteins from the surface to decrease the TIRF signal. This is demonstrated by a simple kinetic model that allows for labeled and unlabeled proteins to displace one another from the surface but does not allow simple desorption:

$$\frac{d\theta_L}{dt} = k_L C_L(1 - \theta_L - \theta_U) - k_{dU} C_U \theta_L + k_{dL} C_L \theta_U, \qquad (22)$$

$$\frac{d\theta_U}{dt} = k_U C_U(1 - \theta_L - \theta_U) + k_{dU} C_U \theta_L - k_{dL} C_L \theta_U. \qquad (23)$$

Here, subscripts L and U represent labeled and unlabeled proteins, respectively, θ is the surface coverage, C is the bulk protein concentration, k_L and k_U are adsorption rate constants, and k_{dL} and k_{dU} are rate constants for labeled proteins displacing unlabeled proteins, and for unlabeled proteins displacing labeled proteins, respectively. Bearing in mind that a fluorescence overshoot would result from a maximum in the labeled protein surface coverage, the model may be summarized as follows: if $k_U \geq k_L$, a fluorescence overshoot will be observed only if $k_{dU} > k_{dL}$ (preferential displacement by unlabeled proteins); if $k_U < k_L$, a fluorescence overshoot will be observed if $k_{dU} \geq k_{dL}$. In other words, fluorescence overshoots still occur when unlabeled proteins preferentially displace labeled proteins, but in this latter case k_{dU} may be *equal* to k_{dL} and still produce an overshoot. Further examination of this case ($k_U < k_L$ and $k_{dU} = k_{dL}$) indicates that it may be ruled out, for it predicts that a fluorescence overshoot should be observed at all labeling ratios at the same time, whereas the data showed that the fluorescence overshoot occurred at progressively longer times for lower labeling ratios (and none was observed for the lowest labeling ratio). Thus, we may be confident that our measurement of the relative quantum yield is not biased by preferential adsorption, and we have made a valid assumption that the average labeling ratios on the surface and in solution are equal.

EFFECT OF CONCENTRATION QUENCHING ON FRAPP MEASUREMENTS

We examined the effect that the degree of concentration quenching measured in the FITC-RNase A systems would have on FRAPP experiments by inserting the empirical $q_r(C)$ relationship 20 into relation 5 and integrating numerically. We used the value of the surface concentration for RNase A adsorbed to polystyrene, 0.22 μg/cm^2, and performed calculations with several different values of the labeling ratio. In this manner we generated theoretical (quenching-influenced) FRAPP recovery curves for arbitrary values of D and f and fitted the theoretical curves with the "inadequate" Eq. 16. This simulated the determination of D and f from experimental data without properly accounting for concentration quenching. The primary consequence of ignoring concentration quenching was to overestimate the mobile

fraction, as illustrated in Fig. 9. This figure plots the incorrect mobile fraction that one would obtain by ignoring concentration quenching versus the correct mobile fraction that was used to generate the theoretical recovery curve. Overestimation of the mobile fraction was severe at higher labeling ratios; in fact it was possible to calculate erroneously a mobile fraction greater than 1. Meanwhile, calculation of D was not affected by this oversight, and the plot shown in Fig. 9 was not affected by the value of D used to generate the recovery curves. (In contrast, the values of both D and f may be significantly altered by concentration quenching for the more commonly employed spot photobleaching configuration. This is discussed in the Appendix.)

The reason why one would overestimate the mobile fraction when using the FRAPP analysis that ignores concentration quenching is best illustrated by inspection of Eq. 17. Before photobleaching, the surface fluorophore concentration is largest, and the quantum yield is at its lowest value. Photobleaching "relieves" some of the concentration quenching, and F_0 is thus unexpectedly large. The denominator in Eq. 17 is thus decreased, and the mobile fraction is overestimated. To determine the mobile fraction from FRAPP experiments, it is critical to measure $\bar{F}$ and F_0 accurately and to relate these accurately to surface concentration profiles.

A related issue is that the full range of the fluorescence recovery, i.e., the difference between $F(\infty)$ and F_0, is compressed by concentration quenching, because of the discrepancy between the relative quantum yields at time zero and infinity. Given noisy FRAPP data and a low mobile fraction, it could be possible for the artificially compressed fluorescence recovery to be obscured by the noise, and one might conclude incorrectly that a sample was completely immobile. This may appear to contradict the preceding discussion of the overestimation of the mobile fraction by ignoring quenching, but this point is solely a matter of signal-to-noise ratio and does not affect the preceding discussion.

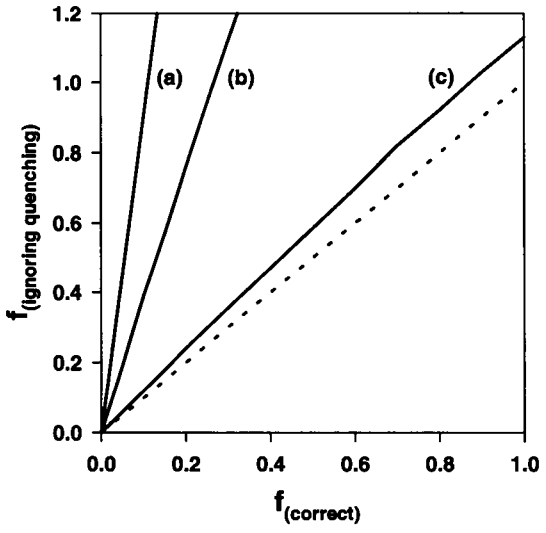

FIGURE 9 Under concentration quenching conditions, the mobile fraction determined by nonlinear regression of FRAPP data to Eq. 16, $f_{(\text{ignoring quenching})}$, significantly overestimates the correct mobile fraction, $f_{(\text{correct})}$. (*a*) $L = 0.20$, (*b*) $L = 0.10$, (*c*) $L = 0.04$. The dashed curve is $f_{(\text{ignoring quenching})} = f_{(\text{correct})}$. In these calculations, the surface concentration of RNase A is 0.22 $\mu g/cm^2$.

The seemingly obvious solution to the problem of concentration quenching is to use low labeling ratios to increase the average interfluorophore separation in FRAP experiments. Unfortunately, this may decrease the signal-to-noise ratio unacceptably in the recovery curves. This is particularly important in two-dimensional systems. Even though a monolayer may be closely packed, it contains very few molecules and hence emits a low-intensity fluorescence signal (particularly when the excitation light must be limited to very low intensity to avoid photobleaching during the recovery). This may make the use of low labeling ratios impractical. If one is forced to use a higher labeling ratio to obtain a satisfactory signal-to-noise ratio, one may also be forced to accept the consequences of close molecular packing: efficient energy transfer and concentration quenching. In these situations, one must determine the concentration dependence of the relative quantum yield and analyze the FRAP results according to relation 3 (or 5).

We wish to emphasize that Fig. 9 is not a universal correction chart. It is intended only to illustrate the influence of concentration quenching, and it is specific to the FRAPP experiments in this study. Relation 3 is universally applicable to FRAP experiments.

Since concentration quenching was significant for adsorbed FITC-RNase A at larger labeling ratios, we used relation 5 and the $q_r(C)$ relationship of relation 20 to analyze the FRAPP data for a labeling ratio of 0.04. We thus determined that $D = (4.9 \pm 0.7) \times 10^{-8}$ cm^2/s and $f = 0.14 \pm 0.04$ for RNase A adsorbed at 0.22 $\mu g/cm^2$ on polystyrene. FRAPP measurements with FITC-RNase A at higher labeling ratios were generally obscured by the noise because of the artificial compression of the range of fluorescence intensities spanned during the recovery, combined with the low mobile fraction, as discussed above. In cases where recoveries at high labeling ratios were obscured by concentration quenching, a repeat photobleaching of the same region on the surface provided measurable fluorescence recovery curves, owing to the partial relief of concentration quenching provided by the first photobleach. The poor signal-to-noise ratio for FITC-RNase A adsorbed to PDMS at pH 6, a result of the pH quenching of fluorescein, prevented reliable FRAPP measurements in that system.

Inasmuch as FITC-BSA did not display concentration quenching in the range of labeling ratios used in our experiments, we determined its diffusion coefficient and mobile fraction simply by fitting FRAPP data to Eq. 16. We found $D = (8 \pm 2) \times 10^{-9}$ cm^2/s and $f = 0.28 \pm 0.03$ for BSA adsorbed at 0.15 $\mu g/cm^2$ on polystyrene. A more complete exploration of surface diffusion in these systems is deferred to another study.

CONCLUSIONS

Although it may not be readily detectable in fluorescence recovery curves, concentration quenching can have a large

effect on the correct interpretation of FRA(P)P data. The appearance of a TIRF signal overshoot during adsorption of labeled proteins at the solid–liquid interface alerted us to the presence of concentration quenching in two of our experimental systems. Aware of the problem, we were then able to measure the concentration dependence of the relative quantum yield of adsorbed FITC-RNase A to correct the FRAPP analysis method. In the case of fringe pattern photobleaching, neglect of concentration quenching generally will lead to overestimation of the mobile fraction, with no effect on the calculated value of the diffusion coefficient. The exception is a system having a low mobile fraction and a low signal-to-noise ratio, in which case the entire recovery may be obscured by the tendency of concentration quenching to compress the range of the fluorescence recovery. This would lead to the incorrect conclusion that all species were completely immobile. In the case of spot photobleaching measurements, both the diffusion coefficient and the mobile fraction may be in error if concentration quenching is present but ignored.

The mobile fraction is an important parameter in describing the lateral mobility of biomolecules, as it may indicate varying degrees of external constraints on the molecules, such as cytoskeletal contacts or two-dimensional aggregation in the case of membrane proteins. Descriptive conclusions could therefore be in error if the mobile fraction were incorrectly calculated from FRA(P)P data. Our current comparison of RNase A and BSA suggests that this problem may be more severe with smaller proteins.

Although it currently is not standard practice to report labeling conditions in the literature, it is possible that other systems under study by FRA(P)P may suffer from undetected concentration quenching. We had the advantage of being alerted to concentration quenching by monitoring adsorption kinetics with TIRF, but this will not be possible in many applications of FRA(P)P. We recommend that labeling conditions be quantified and that FRA(P)P studies be preceded by a quantitative examination of the concentration dependence of the relative quantum yield.

APPENDIX: SPOT PHOTOBLEACHING

Fringe pattern photobleaching is less commonly applied than spot photobleaching, where the illumination profile typically is Gaussian. Here we present sample calculations showing that errors in both D and f may result from concentration quenching in the spot photobleaching geometry. After photobleaching with a circular, Gaussian laser beam having the intensity profile

$$I(r) = \frac{2P}{\pi R^2}\exp\left(-\frac{2r^2}{R^2}\right), \tag{24}$$

the unbleached fluorophore concentration profile relaxes according to

$$C(r,t) = \bar{C}\sum_{n=0}^{\infty}\frac{(-k)^n}{n!}\left(\frac{R^2}{R^2+8nDt}\right)\exp\left[-\frac{2nr^2}{8nDt+R^2}\right]. \tag{25}$$

In Eqs. 24 and 25, R is the Gaussian radius of the incident laser beam, P is the laser power, C is the uniform fluorophore concentration before photobleaching, and k is the depth of photobleaching parameter. We substitute Eqs. 24 and 25 into relation 3 to generate the fluorescence recovery. Just as in the case of fringe pattern photobleaching, we again account for the varying relative quantum yield by substituting relation 20 into relation 3. (Relation 20 is independent of the photobleaching geometry.) In Fig. 10 fluorescence recoveries that were generated for $D = 6.25 \times 10^{-8}$ cm^2/s, $f = 0.30$, and $k = 3.25$ are plotted as a function of the dimensionless time (t/τ_D, where $\tau_D = R^2/4D$). Curves corresponding to a FITC-RNase A surface concentration of 0.2 μg/cm^2 at labeling ratios of $L = 0.04$, 0.10, and 0.25 are presented, along with the recovery that would be obtained in the absence of concentration quenching. It is evident not only that the extent of the recovery is altered but that the kinetics of the recovery appear to be accelerated by increasing degrees of concentration quenching. The relatively rapid decrease in q_r during the recovery at higher labeling ratios has the effect of prematurely truncating the recovery, resulting in the appearance of a more rapid recovery. Table 1 presents the values of D and f that we obtained by analyzing these fluorescence recoveries without considering concentration quenching, along with the apparent value of the bleaching parameter k necessary for the analysis.

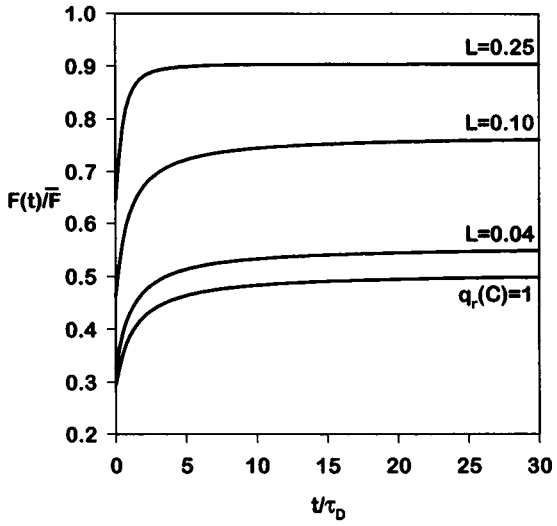

FIGURE 10 Fluorescence recovery after spot photobleaching curves are distorted by fluorescence concentration quenching. All the curves were generated with $k = 3.25$, $D = 6.25 \times 10^{-8}$ cm^2/s, and $f = 0.3$, but the kinetics and extent of the recovery appear exaggerated by higher degrees of concentration quenching (larger values of L). The bottom curve, labeled $q_r(C) = 1$, is the fluorescence recovery that would be obtained in the absence of concentration quenching.

The curves shown in Fig. 10 represent just one set of possibilities. Unlike those for fringe pattern photobleaching, which maintained the characteristic single exponential shape, spot photobleaching recovery curves may display a variety of shapes that deviate systematically from the expected functional form, depending on the labeling ratio, depth of photobleaching, mobile fraction, etc. Some systematic deviations may mimic the effect of a flow superimposed upon the diffusional transport, and it may be possible for the recovery curves to display shoulders and/or overshoots before the full fluorescence recovery, particularly in the case of deeper photobleaching at larger fluorophore concentrations.

TABLE 1 Standard analysis of fluorescence recoveries after spot photobleaching in the presence of concentration quenching

L	D (cm^2/s)	f	k (Apparent)
0.25	3.1×10^{-7}	0.73	0.95
0.10	9.1×10^{-8}	0.57	1.81
0.04	6.9×10^{-8}	0.34	2.88
No quenching (correct values)	6.25×10^{-8}	0.30	3.25

We thank Prasad N. S. B. and Eric Furst for assistance with the scanning angle reflectometry measurements in our laboratory and Jane Tong for her participation in developing the FRAPP instrumentation and for discussions of spot photobleaching. This work was supported in part by a DuPont Young Faculty Award.

REFERENCES

Abney, J. R., B. A. Scalettar, and N. L. Thompson. 1992. Evanescent interference patterns for fluorescence microscopy. *Biophys. J.* 61:542–552.

Axelrod, D., D. E. Koppel, J. Schlessinger, E. Elson, and W. W. Webb. 1976. Mobility measurement by analysis of fluorescence photobleaching recovery kinetics. *Biophys. J.* 16:1055–1069.

Burghardt, T. P., and Axelrod, D. 1981. Total internal reflection/fluorescence photobleaching recovery study of serum albumin adsorption dynamics. *Biophys. J.* 33:455–468.

Cheng, Y. L., S. A. Darst, and C. R. Robertson. 1987. Bovine serum albumin adsorption and desorption rates on solid surfaces with varying surface properties. *J. Colloid Interface Sci.* 118:212–223.

Elson, E. L. 1985. Fluorescence correlation spectroscopy and photobleaching recovery. *Ann. Rev. Phys. Chem.* 36:379–406.

Elson, E. L. 1986. Fluorescence photobleaching and correlation spectroscopy for translational diffusion in biological systems. *Biochem. Soc. Trans.* 14:839–841.

Förster, Th. 1959. Transfer mechanisms of electronic excitation. *Disc. Faraday Soc.* 27:7–17.

Fruchter, R. G., and A. M. Crestfield. 1965. Preparation and Properties of two active forms of ribonuclease dimer. *J. Biol. Chem.* 240:3868–3882.

Fung, B. K., and L. Stryer. 1978. Surface density determination in membranes by fluorescence energy transfer. *Biochemistry.* 17:5241–5248.

Gaspers, P. B., C. R. Robertson, and A. P. Gast. 1994. Enzymes on immobilized substrate surfaces: diffusion. *Langmuir.* 10:2699–2704.

Golan, D. E., and W. Veatch. 1980. Lateral mobility of band 3 in the human erythrocyte membrane studied by fluorescence photobleaching recovery: evidence for control by cytoskeletal interactions. *Proc. Natl. Acad. Sci. USA.* 77:2537–2541.

Jacobson, K., and J. Wojcieszyn. 1984. The translational mobility of substances within the cytoplasmic matrix. *Proc. Natl. Acad. Sci. USA.* 81: 6747–6751.

Koppel, D. E. 1986. Fluorescence photobleaching recovery techniques for translational and slow rotational diffusion in solution and on cell surfaces. *Biochem. Soc. Trans.* 14:842–845.

Lok, B. K., Y. L. Cheng, and C. R. Robertson. 1983a. Total internal reflection fluorescence: A technique for examining interactions of macromolecules with solid surfaces. *J. Colloid Interface Sci.* 91:87–103.

Lok, B. K., Y. L. Cheng, and C. R. Robertson. 1983b. Protein adsorption on crosslinked polydimethylsiloxane using total internal reflection fluorescence. *J. Colloid Interface Sci.* 91:104–116.

Norde, W., and J. Lyklema. 1978. The adsorption of human plasma albumin and bovine pancreas ribonuclease at negatively charged polystyrene surfaces. *J. Colloid Interface Sci.* 66:257–265.

Pachence, J. M., S. Amador, G. Maniara, J. Vanderkooi, P. L. Dutton, and J. K. Blasie. 1990. Orientation and lateral mobility of cytochrome *c* on the surface of ultrathin lipid multilayer films. *Biophys. J.* 58:379–389.

Rabe, T. E., and R. D. Tilton. 1993. Surface diffusion of adsorbed proteins in the vicinity of the substrate glass transition temperature. *J. Colloid Interface Sci.* 159:243–245.

Schaaf, P., P. Déjardin, and A. Schmitt. 1987. Reflectometry as a technique to study the adsorption of human fibrinogen at the silica/solution interface. *Langmuir.* 3:1131–1135.

Smith, B. A. 1982. Measurement of diffusion in polymer films by fluorescence redistribution after pattern photobleaching. *Macromolecules.* 15:469–472.

Smith, L. M., J. W. Parce, B. A. Smith, and H. M. McConnell. 1979. Antibodies bound to lipid haptens in model membranes diffuse as rapidly as the lipids themselves. *Proc. Natl. Acad. Sci. USA.* 76:4177–4179.

Snyder, B., and E. Freire. 1982. Fluorescence energy transfer in two dimensions. *Biophys. J.* 40:137–148.

Stryer, L. 1978. Fluorescence energy transfer as a spectroscopic ruler. *Ann. Rev. Biochem.* 47:819–846.

Thompson, N. L., T. P. Burghardt, and D. Axelrod. 1981. Measuring surface dynamics of biomolecules by total internal reflection fluorescence with photobleaching recovery or correlation spectroscopy. *Biophys. J.* 33:435–454.

Tilton, R. D., C. R. Robertson, and A. P. Gast. 1990a. Lateral diffusion of bovine serum albumin adsorbed at the solid-liquid interface. *J. Colloid Interface Sci.* 137:192–203.

Tilton, R. D., A. P. Gast, and C. R. Robertson. 1990b. Surface diffusion of interacting proteins: Effect of concentration on the lateral mobility of adsorbed bovine serum albumin. *Biophys. J.* 58:1321–1326.

Tilton, R. D. 1991. Surface diffusion and hydrophobic interactions in protein adsorption, Ph.D. dissertation. Stanford University, Stanford, CA.

Weis, R. M., K. Balakrishnan, B. A. Smith, and H. M. McConnell. 1982. Stimulation of fluorescence in a small contact region between rat basophil leukemia cells and planar lipid membrane targets by coherent evanescent radiation. *J. Biol. Chem.* 257:6440–6445.

Wolber, P. K., and B. S. Hudson. 1979. An analytic solution to the Förster energy transfer problem in two dimensions. *Biophys. J.* 28:197–210.

Wright, L. L., A. G. Palmer III, and N. L. Thompson. 1988. Inhomogeneous translational diffusion of monoclonal antibodies on phospholipid Langmuir–Blodgett films. *Biophys. J.* 54:463–470.